Limiting precision of tomographic phase estimation

Andrei Tokovinin and Elise Viard

European Southern Observatory, Karl-Schwarzschild-Strasse, 2 D-85748 Garching bei München, Germany

Received April 26, 2000; revised manuscript received September 11, 2000; accepted November 2, 2000

In the context of multiconjugate adaptive optics, the optimum linear estimation of a wave-front phase for a target object using the phases of several surrounding natural guide stars (NGS's) is studied. A Wiener-filter-type estimator is constructed. The minimum residual wave-front-phase (tomographic) error depends on the turbulence vertical profile, and for typical profiles it is almost insensitive to the presence of strong layers, contrary to current belief. Tomographic error is characterized by a new parameter δ_K, equivalent profile thickness, which depends on the NGS number K (typically $\delta_5 = 0.5$ km). The angular radius of the NGS configuration must not exceed r_0/δ_K. Exact profile knowledge is not required. When the optimized filters are constructed from some model profile, the loss of the field size is within 10% with respect to exact profile knowledge. Moreover, a method to measure turbulence profile using wave-front-sensor data is outlined. Noise propagation in the restoration algorithm is significant, but not dramatic. Noise increases with increasing size of NGS constellation. Practically, guide stars for tomography should be at least as bright as those for classical adaptive optics. © 2001 Optical Society of America

OCIS codes: 010.0010, 010.1080, 010.1330.

1. PROBLEM LAYOUT

The idea of multi-conjugate adaptive optics (MCAO) appears first in the studies of Dicke[1] and Beckers.[2] The method of measuring the three-dimensional atmospheric phase perturbations for MCAO was proposed by Tallon and Foy[3] and was called turbulence tomography. The problem of reconstructing the instantaneous perturbations was then regarded as a solution of a set of linear algebraic equations. Turbulence was assumed to be concentrated in a small number of thin layers.

More advanced theories were developed by Johnston and Welsh,[4] Ellerbroek,[5] and, further, by Fusco *et al.*[6] In these studies the statistics of atmospheric phase and measurement noise was taken into account. Fusco *et al.* admit that real turbulence may not be concentrated in a few layers but rather is distributed continuously with altitude. Still, they try to estimate phase distribution in a few equivalent layers and use the formalism of statistical theory (maximum *a posteriori*) to derive the algorithm. These layers are then assumed to be corrected by the corresponding number of deformable mirrors (DM's). *A priori* information on turbulence statistics is used in the form of the covariance matrix of Zernike coefficients and the strengths of equivalent layers. Thus statistical techniques of MCAO optimization need second-order quantities (covariances), unlike the matrix-inversion technique of Tallon and Foy.[3]

In Ref. 7 we investigated the fundamental limits of the field-of-view (FOV) size when correcting real turbulence profiles by a finite number of DM's. The three-dimensional phase distribution was assumed to be known. Correction-limited FOV was characterized by the generalized isoplanatic angle θ_M, a system-independent parameter.

Here we turn to the problem of measuring the wave-front phase using data from several natural guide stars. The number of sources is limited, while the number of turbulent layers is large or infinite. It is thus out of the question to reconstruct the three-dimensional turbulence, because the number of unknowns is much larger than the number of measurements. Instead we are in the realm of statistical theory, trying to find the best possible estimate of the object wave-front phase from the noisy measurements of guide stars. The term "tomography" is used here in this sense. It has been demonstrated experimentally by Ragazzoni *et al.*[8] that such an estimate of the object phase can be obtained by a linear combination of phases measured on neighboring guide stars. Those authors used Zernike decomposition and obtained the desired linear restorator as tomographic matrix. In the present work the precision of such linear restoration is investigated theoretically using Fourier formalism.

We consider an idealized case of a telescope with infinite aperture that observes several natural guide stars (NGS's). Hence, all effects of incomplete beam overlap in the upper atmospheric layers and of wave-front scaling in the case of laser guide stars are outside the scope of this work. These effects are likely to degrade the performance; hence the limits derived below are optimistic for real systems. The problem is illustrated in Fig. 1.

Of course, the idealized problem considered here does not take into account all aspects of future MCAO systems. However, owing to the complexity of MCAO, we feel that it is instructive to consider the fundamental limits by isolating specific factors in idealized models. A different approach—more comprehensive modeling of representative cases—as adopted by other authors, provides more precise performance metric but makes it difficult to disentangle individual factors and explore the limits. Additional interest of this work lies in its relevance to very

 © 2001 Optical Society of America

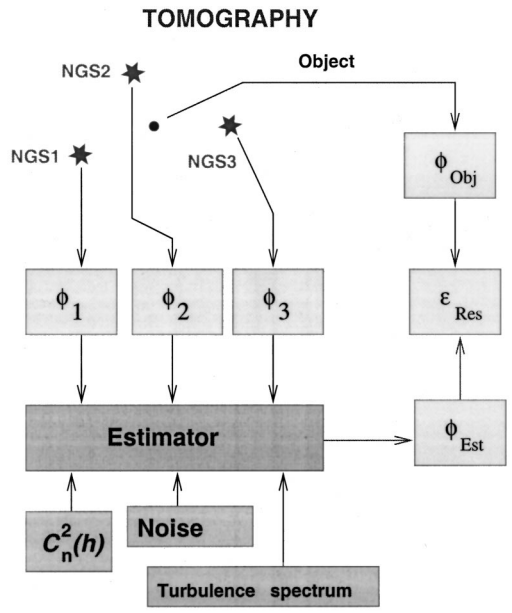

Fig. 1. Problem layout. The phase of the object wave-front ϕ_{Obj} is estimated from the phases of the surrounding guide stars ϕ_i in an optimized way, with use of the *a priori* information on turbulence profile, noise and turbulence statistics. Variance of the residual phase ϵ_{Res} is used as an optimization creterion and as a characteristic of tomographic error.

large apertures, permitting us to estimate MCAO performance on extremely large telescopes.[9]

In Section 2 the theory of optimum linear phase estimation is given. In Section 3 the scaling law of the tomographic error is established, and the new parameter δ_K (equivalent thickness of atmosphere) is introduced. In Section 4 this parameter is computed for a variety of real turbulence profiles, and the sensitivity of reconstruction to exact profile knowledge is studied. A method to estimate turbulence profile from the wave-front-sensor data, eliminating the need for a separate profile monitor, is outlined in Section 5. Noise propagation issues are addressed in Section 6, and conclusions are given in Section 7.

2. THEORY

A. Propagation

A theory of optical propagation through the atmosphere, as reviewed by Roddier,[10] is used throughout this paper. As usual, diffraction effects are neglected, and a simple geometric propagation model is adopted. The scientific target (source) is observed at a direction $\boldsymbol{\theta}$ ($\boldsymbol{\theta} = 0$ is the FOV center).

The atmosphere is composed of a very large number of turbulent layers. One (nth) turbulent layer at an altitude h_n introduces a phase perturbation $\phi_n(\mathbf{r})$. The combined effect of N atmospheric layers leads to the wave-front phases $\phi(\mathbf{r}, \boldsymbol{\theta})$, which depend on the coordinate vector $\mathbf{r}$ and the source position vector $\boldsymbol{\theta}$:

$$\phi(\mathbf{r}, \boldsymbol{\theta}) = \sum_{n=1}^{N} \phi_n(\mathbf{r} - \boldsymbol{\theta} h_n). \tag{1}$$

We denote by tilde the Fourier transforms and recast Eq. (1) in the spatial frequency domain. Spatial shifts translate into exponential factors:

$$\tilde{\phi}(\mathbf{f}, \boldsymbol{\theta}) = \sum_{n=1}^{N} \tilde{\phi}_n(\mathbf{f}) \exp(-2\pi i \mathbf{f}\boldsymbol{\theta} h_n), \tag{2}$$

where the dot product $\mathbf{f} \cdot \boldsymbol{\theta}$ is written simply as $\mathbf{f}\boldsymbol{\theta}$.

B. Wave-Front Sensor

In any real adaptive optics (AO) system a finite number of parameters is measured by a wave front sensor (WFS), and a finite number of wave-front parameters (modes) is corrected. Here we describe the operation of an MCAO system by continuous functions. Following Rigaut *et al.*,[11] the WFS is modeled as a linear filter; the WFS signal is equal to filtered phase plus noise. Unlike Rigaut *et al.*, we neglect the discrete WFS sampling; it amounts to neglecting the aliasing noise, which is not dominating in real systems. In the Fourier domain WFS filtering corresponds to a multiplication by some measurement operator $\mathcal{M}$. For example, a Shack–Hartmann (S–H) WFS measures phase slopes (in units of radians per m) averaged over square subapertures of size d. There are two operators $\mathcal{M}$ for x and y slopes. Slope measurement in the x direction corresponds to

$$\mathcal{M}_x(\mathbf{f}) = 2\pi i f_x \operatorname{sinc}(df_x)\operatorname{sinc}(df_y). \tag{3}$$

The number of guide stars is K, and their positions on the sky are $\boldsymbol{\theta}_k$. Slopes measured in x and y directions are considered separately (see below). The input data for a kth guide star are S_k:

$$S_k(\mathbf{f}) = \mathcal{M}(\mathbf{f})\tilde{\phi}(\mathbf{f}, \boldsymbol{\theta}_k) + \tilde{\nu}_k(\mathbf{f}), \tag{4}$$

where $\tilde{\nu}_k$ is the noise term.

In reality a WFS measures wave fronts only within the telescope pupil. Multiplication by a pupil window function leads to a convolution in Fourier space, which is not described by Eq. (4). The theory presented below is hence applicable to very large apertures (AO systems of high order), when edge effects may be neglected.

The power spectral density of photon noise in a S–H WFS may be written as

$$\nu_k^2(\mathbf{f}) = (2\pi/\lambda)^2 \alpha^2 N^{-1} \operatorname{sinc}^2(df_x)\operatorname{sinc}^2(df_y), \tag{5}$$

where α is the spot size and N is the photon flux density on the subapertures, in photons per square meter. This is white noise filtered with square subapertures. When integrated over frequencies, this spectrum gives the correct slope variance of $(2\pi/\lambda)^2\alpha^2/(Nd^2)$.

C. Linear Estimator and Residual Phase Error

Given a set of WFS measurements, we want to determine the best linear estimate of the phase $\tilde{\psi}(\mathbf{f}, \boldsymbol{\theta})$ for the viewing direction $\boldsymbol{\theta}$. The most general form of a linear estimator is a sum of suitably weighted and filtered WFS measurements:

$$\tilde{\psi}(\mathbf{f}, \boldsymbol{\theta}) = \sum_{k=1}^{K} g_k(\mathbf{f}, \boldsymbol{\theta}) S_k(\mathbf{f}). \tag{6}$$

The difference ϵ between real and estimated phases can be computed as a combination of atmospheric phases, summed over all layers, and noise:

$$\tilde{\epsilon}(\mathbf{f}, \boldsymbol{\theta}) = \tilde{\phi} - \tilde{\psi} = \sum_{n=1}^{N} P(\mathbf{f}, \boldsymbol{\theta}, h_n)\tilde{\phi}_n(\mathbf{f}) - \sum_{k=1}^{K} g_k(\mathbf{f}, \boldsymbol{\theta})\tilde{\nu}_k(\mathbf{f}), \tag{7}$$

where the filter P is equal to

$$P(\mathbf{f}, \boldsymbol{\theta}, h) = \exp(-2\pi i \mathbf{f}\boldsymbol{\theta}h)\left\{1 - \sum_{k=1}^{K} g_k(\mathbf{f}, \boldsymbol{\theta})\mathcal{M}(\mathbf{f}) \times \exp[2\pi i \mathbf{f}(\boldsymbol{\theta} - \boldsymbol{\theta}_k)h]\right\}. \tag{8}$$

D. Residual Power Spectrum

The power spectrum of the residual phase can now be derived from the power spectra of phase and noise terms. The power spectrum of atmospheric phase W_ϕ is given by the Kolmogorov model. The Von Kármán model with finite outer scale can be used instead, but, as we shall see, the low-frequency part of the spectrum does not influence the result. Therefore, the use of Kolmogorov model is not restrictive. It is convenient to isolate the refractive index structure constant $C_n^2(h)$ by writing for the nth layer

$$W_\phi(\mathbf{f}) = W_0(\mathbf{f})C_n^2(h_n)\mathrm{d}h, \tag{9}$$

$$W_0(\mathbf{f}) = 9.69 \times 10^{-3}(2\pi/\lambda)^2|\mathbf{f}|^{-11/3}. \tag{10}$$

The usual assumptions are now made. Phase perturbations in individual layers are mutually independent. Noise contributions in different sources are mutually independent. Noise is not correlated with phase. All this permits us to express the power spectrum of residual phase as a sum of individual power spectra. The sum of atmospheric terms is written, naturally, as an integral over altitude (integration limits are not explicitly given, being defined by the atmosphere extent):

$$W_\epsilon(\mathbf{f}) = W_0(\mathbf{f})\int |P(\mathbf{f}, \boldsymbol{\theta}, h)|^2 C_n^2(h)\mathrm{d}h + \sum_{k=1}^{K} |g_k(\mathbf{f}, \boldsymbol{\theta})|^2 \nu_k^2(\mathbf{f}), \tag{11}$$

where $\nu_k^2(\mathbf{f})$ is the noise power spectrum for the kth guide star, and the spatial filter $|P|^2$ is given by

$$|P(\mathbf{f}, \boldsymbol{\theta}, h)|^2 = 1 - 2\,\mathrm{Re}\sum_{k=1}^{K} g_k\mathcal{M}\exp[2\pi i \mathbf{f}(\boldsymbol{\theta} - \boldsymbol{\theta}_k)h] + \sum_{k=1}^{K}\sum_{k'=1}^{K} g_k g_{k'}^* |\mathcal{M}|^2 \exp[2\pi i \mathbf{f}(\boldsymbol{\theta}_{k'} - \boldsymbol{\theta}_k)h]. \tag{12}$$

Here Re means real part, * means complex conjugate, and $\mathbf{f}, \boldsymbol{\theta}$ arguments of g_k and $\mathcal{M}$ are omitted.

AO imaging properties do not depend on the constant-phase component within the telescope aperture, the piston. The power spectrum of piston-removed phase residuals can be computed in the same way by introducing into Eq. (11) an additional filtering term that depends on aperture size, as done in Ref. 7. This term reduces the contribution of low spatial frequencies, which is not significant for this particular problem, just as outer scale. We do not include the piston term in the following formulas, which are then correct in the limit of infinitely large aperture, when the piston can be neglected.

The altitude dependence of $|P|^2$ is given by phase terms of the type $\exp(2\pi i \xi h)$. When multiplied by $C_n^2(h)$ and integrated over altitude, this leads to the Fourier transform of the turbulence profile, $\tilde{C}(\xi)$:

$$\tilde{C}(\xi) = \int C_n^2(h)\exp(2\pi i \xi h)\mathrm{d}h. \tag{13}$$

Thus the turbulence vertical profile enters only through its Fourier transform.

For brevity, in the following formulas we do not write explicitly the frequency and angular arguments. Using Eq. (12), we express the integrals over altitude through $\tilde{C}$. This leads to

$$W_\epsilon = W_0 c_0\left(1 - 2\,\mathrm{Re}\sum_{k=1}^{K} g_k c_k + \sum_{k=1}^{K}\sum_{k'=1}^{K} g_k g_{k'}^* a_{kk'} + \sum_{k=1}^{K} |g_k|^2 \nu'_k\right), \tag{14}$$

where

$$c_0 = \tilde{C}(0),$$
$$c_k = \mathcal{M}\tilde{C}[\mathbf{f}(\boldsymbol{\theta} - \boldsymbol{\theta}_k)]/c_0,$$
$$a_{kk'} = |\mathcal{M}|^2\tilde{C}[\mathbf{f}(\boldsymbol{\theta}_{k'} - \boldsymbol{\theta}_k)]/c_0,$$
$$\nu_k' = \nu_k^2/(W_0 c_0). \tag{15}$$

The matrix $\mathbf{A} = \{a_{kk'}\}$ is Hermitian, $a_{kk'} = a_{k'k}^*$, and W_ϵ is real. Only the vector $\mathbf{c}$ depends on source position $\boldsymbol{\theta}$. The parameter c_0 is the integral of the turbulence profile related to the Fried parameter r_0:

$$c_0 = \frac{6.88}{2.91}\left(\frac{\lambda}{2\pi}\right)^2 r_0^{-5/3}. \tag{16}$$

For the S–H WFS the number of measurements (and hence matrix dimensions) K is twice the number of guide stars, so K in the above formulas is doubled. The slopes in x and y directions are mutually correlated for noncoincident subapertures, leading to some nonzero elements of the matrix $\mathbf{A}$ corresponding to xy combinations. However, we neglect this correlation and consider the slope components separately by setting the xy elements of $\mathbf{A}$ to zero. We verified that in the low-noise case this treatment leads to the same results as the direct measurement of phase ($\mathcal{M} = 1$).

It is instructive to look at the dimensions of the relevant quantities. Phase is dimensionless, and its slope (and hence $\mathcal{M}$) is measured in inverse meters, and its power spectrum W_ϵ in square meters. Filters g_k, which transform slopes to phases, are in meters. Vector $\mathbf{c}$ is measured in $\mathrm{m}^{-2/3}$, matrix $\mathbf{A}$ and vector ν' in $\mathrm{m}^{-5/3}$, and c_0 in $\mathrm{m}^{1/3}$.

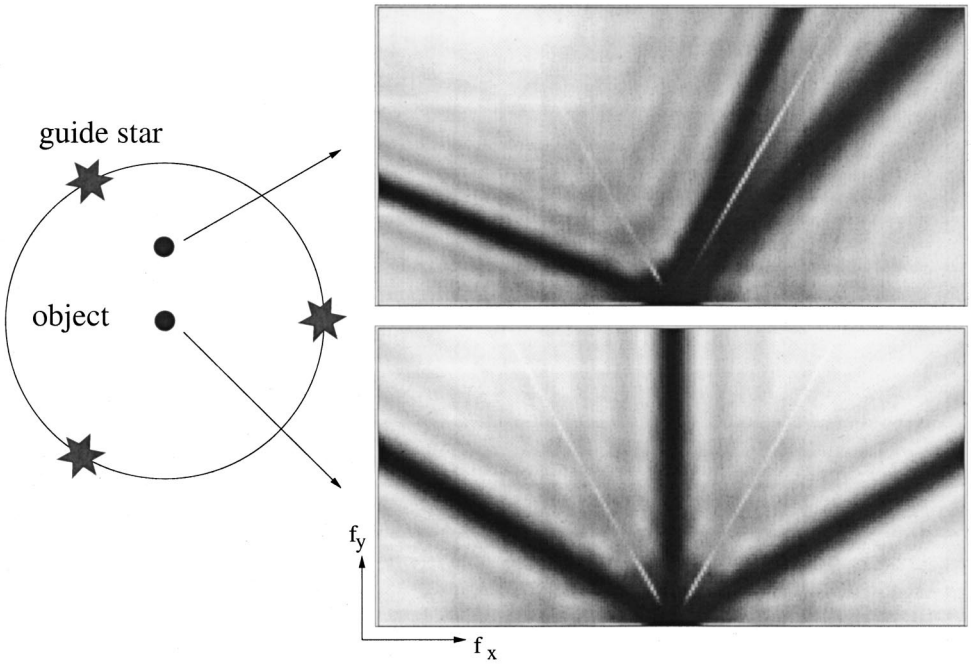

Fig. 2. Error transfer function $G(\mathbf{f})$ in the spatial frequency plane (right) for three guide stars and two positions of object: at the FOV center and decentered. The Paranal model profile (see Section 4) was used in the calculations. Only the upper half of the frequency plane is displayed owing to symmetry; coordinate origin is in the middle of the f_x axis. Dark shadows are perpendicular to the directions for which the object projects onto one of the guide stars. Bright stripes at $\pm 30°$ from vertical correspond to the directions for which matrix $\mathbf{A}$ would be singular without measurement noise; in these directions the error-transfer function depends on the adopted noise level.

E. Optimization

The filters g_k can be found that minimize W_ϵ at any spatial frequency $\mathbf{f}$ and for a particular viewing direction $\boldsymbol{\theta}$. This would ensure the minimization of the residual phase variance. This derivation follows the idea of the Wiener filter, which is obtained as a linear filter minimizing the rms difference between restored and original signals, as explained in Ref. 12.

We differentiate Eq. (14) over real and complex parts of g_k and solve the resulting system of equations. The answer, in a compact matrix form, is

$$\mathbf{g} = [(\mathbf{A} + \nu' \mathbf{I})^{-1} \mathbf{c}]^*, \tag{17}$$

where $\mathbf{I}$ is the unity matrix. The presence of even a small amount of noise guarantees the existence of the inverse matrix and makes the problem numerically stable. Otherwise the simple configurations with few layers lead to a singular matrix $\mathbf{A}$ at some frequencies, when relative shifts of phase screens of some pair of NGS's happen to be equal (or different by $2\pi n$) and hence do not contain independent information. Combining the expressions given above, the relative noise power ν' (wavelength independent) is given by

$$\nu'(\mathbf{f}) = 103.2 \alpha^2 N^{-1} c_0^{-1} |\mathbf{f}|^{11/3} \operatorname{sinc}^2(df_x) \operatorname{sinc}^2(df_y). \tag{18}$$

When the optimum filters are found, they can be put back into Eq. (14) to obtain the power spectrum of residual wave-front errors. It is instructive to write explicitly the error transfer function $G(\mathbf{f}, \boldsymbol{\theta})$ as

$$G(\mathbf{f}, \boldsymbol{\theta}) = 1 - 2 \operatorname{Re}(\mathbf{c}^T \mathbf{g}) + \mathbf{g}^T \mathbf{A} \mathbf{g}^* \tag{19}$$

and to express the residual spectrum as

$$W_\epsilon(\mathbf{f}) = c_0 W_0(\mathbf{f}) [G + \mathbf{g}^T (\nu' \mathbf{I}) \mathbf{g}^*]. \tag{20}$$

The low-frequency components of phase spectrum experience small relative phase delays $\exp[2\pi i \mathbf{f}(\boldsymbol{\theta} - \boldsymbol{\theta}_k)h]$ and hence will be well estimated from NGS phases. One would expect that at low frequencies G is close to zero. Then G grows and eventually reaches 1, which means a complete absence of information on high spatial frequencies, because the NGS phase becomes decorrelated with the object wave-front phase.

Using the fact that both $\mathbf{A}$ and $(\mathbf{A} + \nu' \mathbf{I})^{-1}$ are Hermitian, and neglecting noise, we may simplify the error transfer function with optimum filters to

$$G'(\mathbf{f}, \boldsymbol{\theta}) \approx 1 - \mathbf{c}^T \mathbf{A}^{-1} \mathbf{c}^*. \tag{21}$$

However, to study the sensitivity of phase reconstruction to the exact knowledge of a profile, we must calculate $\mathbf{g}$ using our best idea of the profile and then substitute the real profile into $\mathbf{A}$ and $\mathbf{c}$ and compute phase residuals using the full Eq. (19), not Eq. (21).

In Fig. 2 the two-dimensional shape of the error transfer function is given for a symmetrical configuration of three guide stars and a model turbulence profile, for two object positions. The function goes to zero at low spatial frequencies and also for several directions orthogonal to the directions where the object projects onto some of the guide stars. In these directions the Fourier components of the object wave front are in phase with NGS wave fronts and hence are well measured. One may think of the zeros in $G(\mathbf{f})$ as shadows cast by turbulent layers. When the turbulence profile is compressed in altitude, the

shadows get wider and residual variance diminishes. For profiles with several thin layers, the structure of shadows is more complex.

3. SCALING LAW FOR TOMOGRAPHIC ERROR

How precisely can the object phase be reconstructed? To answer this question, we assume that wave fronts of guide stars are measured directly [$\mathcal{M}(\mathbf{f}) = 1$] and without noise ($\nu' = 0$). In this case the optimum filters g_k and the error transfer function $G_K(\mathbf{f}, \boldsymbol{\theta})$ do not depend on the turbulence spectrum but are defined entirely by problem geometry. The subscript K is added to highlight the dependence of G_K on the number of NGS's. It may be verified that G_K is invariant to a profile translation [i.e., to the multiplication of $\tilde{C}(\xi)$ by a factor $\exp(2\pi i \xi x)$] and to a change of turbulent energy (due to the normalization by c_0). Thus the limiting quality of wave-front reconstruction from noiseless data depends only on the source geometry and on the shape of the turbulence profile. The minimum residual phase variance (tomographic error) is obtained by integrating the first term of Eq. (20):

$$\langle \epsilon^2_{\mathrm{tom}}(\boldsymbol{\theta}) \rangle = c_0 \int W_0(\mathbf{f}) G_K(\mathbf{f}, \boldsymbol{\theta}) \mathrm{d}\mathbf{f}. \quad (22)$$

In Fig. 3 the dependence of tomographic phase-error variance on object position is illustrated. Variance is zero when the object is close to one of the guide stars (in this case it depends only on WFS noise).

Now let us establish the scaling law for tomographic phase error, that is, its dependence on the size of the NGS constellation. Let Θ be the distance of NGS's from the FOV center (for complex NGS configurations some mean distance must be used). The change of variables $\boldsymbol{\theta}' = \boldsymbol{\theta}/\Theta$ and $\mathbf{f}' = \mathbf{f}\Theta$ is useful for singling out the dependence of $\langle \epsilon^2_{\mathrm{tom}} \rangle$ on Θ.

Both $\mathbf{c}$ and $\mathbf{A}$ depend on the spatial frequency $\mathbf{f}$ only through the products of the type $\boldsymbol{\theta}\mathbf{f}$ [see Eq. (15)], which means that $G_K(\mathbf{f}, \boldsymbol{\theta}) = G_K(\mathbf{f}', \boldsymbol{\theta}')$. From Eq. (21) it is also clear that when WFS noise can be neglected, G_K is independent of the WFS measurement operators $\mathcal{M}$ because they cancel out in the $\mathbf{c}^T\mathbf{A}^{-1}\mathbf{c}^*$ term. Taking into account the form of W_0, we transform Eq. (22) into

$$\langle \epsilon^2_{\mathrm{tom}}(\boldsymbol{\theta}') \rangle = c_0 \Theta^{5/3} \int W_0(\mathbf{f}') G_K(\mathbf{f}', \boldsymbol{\theta}') \mathrm{d}\mathbf{f}'. \quad (23)$$

It remains to express c_0 through r_0 [Eq. (16)]. Using Eq. (10) and combining constants, we eventually get

$$\langle \epsilon^2_{\mathrm{tom}}(\boldsymbol{\theta}') \rangle = \Theta^{5/3} r_0^{-5/3} \delta_K^{5/3} e_K(\boldsymbol{\theta}'), \quad (24)$$

where

$$\delta_K^{5/3} e_K(\boldsymbol{\theta}') = 0.0229 \int |\mathbf{f}'|^{-11/3} G_K(\mathbf{f}', \boldsymbol{\theta}') \mathrm{d}\mathbf{f}'. \quad (25)$$

The new parameter δ_K has a dimension of length. It depends neither on Θ nor on wavelength (all error dependence on wavelength is contained in r_0, as is typical for many other atmospheric-propagation problems). On the other hand, δ_K depends on the turbulence profile shape and on the NGS configuration. The dimensionless term $e_K(\boldsymbol{\theta}')$ describes the variation of $\langle \epsilon^2_{\mathrm{tom}} \rangle$ across the field, and it is convenient to set $e_K(0) = 1$. Then Eq. (25) can be used to calculate δ_K by setting $\boldsymbol{\theta}' = 0$.

In analogy to the atmospheric isoplanatic patch size[13] θ_0, a tomographic patch size γ_K can now be introduced. When the radius of the K-NGS constellation reaches γ_K, the tomographic error in the center of the FOV equals 1 square radian. At other FOV locations this error can be either smaller or larger, depending on the function $e_K(\boldsymbol{\theta}')$. The size of the corrected FOV in MCAO cannot be much larger than γ_K. It follows from Eq. (24) that

$$\langle \epsilon^2_{\mathrm{tom}}(\boldsymbol{\theta}') \rangle = e_K(\boldsymbol{\theta}') (\Theta/\gamma_K)^{5/3}$$

$$\gamma_K = r_0/\delta_K. \quad (26)$$

The parameter δ_K may be called the effective thickness of the turbulence profile with respect to a given NGS configuration. It describes the interplay between the position and the thickness of the layers and the source geometry. For example, when the layers are infinitely thin and their number is not greater than the number of NGS's, the pure tomographic case is realized, and we obtain $\delta_K = 0$, whatever the layer altitudes. In the opposite case of turbulence uniformly distributed in a layer of thickness L, the δ_K parameter will be directly proportional to L, with the proportionality coefficient depending on the number and positions of NGS's.

This scaling law leads to an interesting consideration about the maximum number of pixels in the corrected image. Image size will be of the order of $2\Theta = 2r_0/\delta_K$, and the pixel size must be $\lambda/2D$ (Nyquist sampling). The number of pixels along one image axis, N_{pixel}, can be estimated as the ratio of these. Taking into account the de-

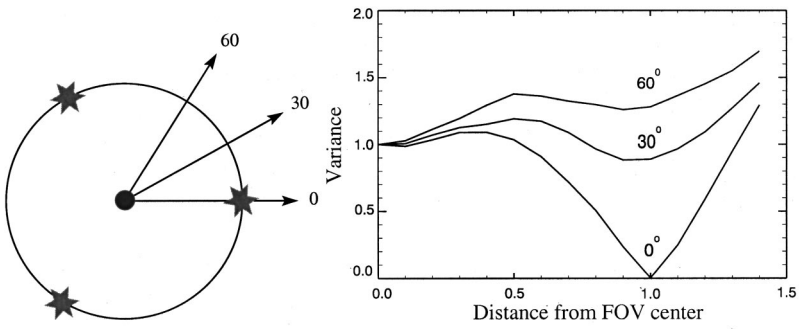

Fig. 3. For a symmetrical configuration of three guide stars the dependence of residual-phase variance on object position is traced when the object is moved from the FOV center in three directions. Object position along the radius is given in units of guide star distance from center.

pendence of r_0 on wavelength, it turns out that N_{pixel} dependence on wavelength is small:

$$N_{\text{pixel}} = \left(\frac{\lambda}{\lambda_0}\right)^{1/5} \frac{4Dr_0(\lambda_0)}{\delta_K \lambda_0}. \quad (27)$$

Assuming $\delta_3 = 1\,\text{km}$ (see below), $\lambda = \lambda_0 = 500\,\text{nm}$, $r_0(\lambda_0) = 0.15\,\text{m}$, and $D = 8\,\text{m}$, we obtain $N_{\text{pixel}} = 9600$. Going to the wavelength of 2.2 μm increases N_{pixel} by only a factor of 1.34. The conclusion is that the detector format for imaging with MCAO at 8-m telescopes is likely to be limited to $8\text{K} \times 8\text{K}$ or $16\text{K} \times 16\text{K}$ if a small number of guide stars is used for tomography.

4. EFFECTIVE THICKNESS FOR REAL TURBULENCE PROFILES

In this section the tomographic error will be quantified, still assuming zero noise and $\mathcal{M} = 1$ case. First we calculate the effective thickness of a uniform turbulence distribution. A variable number of guide stars K was tried in symmetrical configurations about the FOV center. The resulting ratio of the effective thickness δ_K to the layer thickness L is given in Table 1.

The general tendency of δ_K to decrease while K increases is clear. However, it is also seen that symmetrical configurations ($K = 4, 6, 8$) produce slightly worse results than asymmetrical ones ($K = 3, 5$). This is understandable: In symmetrical configurations the number of directions for which the object projects exactly on some of the guide stars is less than K as a result of symmetry. These directions correspond to the minima of the error transfer function $G(\mathbf{f})$ in the frequency plane (shadows). In the following we concentrate on the $K = 3$ and $K = 5$ cases as representative of future MCAO geometry.

The case $K = 1$ deserves additional comment. At first glance, it describes classical anisoplanatism, when the phase difference between object and guide star increases with their increasing separation. Still, here the phase difference does not depend on the layer altitude and, moreover, the object phase is estimated with optimum spatial filtering (with increasing distance from NGS the uncorrelated high-frequency components are progressively removed from the estimated phase). Classical formulas relating the anisoplanatic rms phase difference to atmospheric patch size θ_0[13], when applied to a layer of thickness $L/2$ at altitude zero, would give a result that corresponds to $\delta_1 = r_0/\theta_0 = (6.88 \times 3/8)^{3/5} \times 0.5L = 0.88L$, in comparison with $0.69L$, obtained here with optimized filtering.

For the Hufnagel–Valley turbulence profile[14] one obtains $\delta_3 = 889\,\text{m}$ and $\delta_5 = 554\,\text{m}$ for three and five guide stars, respectively (γ_K of 24.8″ and 39.8″ at 500 nm for $r_0 = 0.107$ m). Comparing those numbers with the uniform-thick-layer model (Table 1), we find that the Hufnagel profile may be assimilated to a 7.5-km-thick uniform turbulent slab. It is interesting that the correction-limited isoplanatic angle was computed in Ref. 7 to be $\theta_3 = 8.4''$ at 500 nm.

Real turbulence profiles often contain few strong layers. One might expect that in this case equivalent width would be smaller. We use the set of 12 $C_n^2(h)$ profiles obtained by balloon soundings at Paranal, Chile.[15,16] Flights 51 and 52 are selected as typical of this data set. They have similar r_0 and θ_0 values, but profile 51 has a well-marked strong layer in addition to the ground layer (Fig. 4). We also use the average Paranal profile. Corresponding equivalent widths for three and five NGS's are given in Table 2.

From Fig. 4 it is clear that at Paranal, turbulence is found at all altitudes. Even when a strong layer is present, the continuous component is nonnegligible. In fact, equivalent thickness of profile 51 is more than that of profile 52 or of the mean profile. We conclude that the presence of strong layers in itself is not enough to improve the quality of phase reconstruction, unless all turbulence is indeed concentrated in a small number of very thin layers.

Inspired by the shape of the Paranal mean profile, we consider a Paranal model profile consisting of only two equally strong thick layers: a 2-km layer at mean altitude of 1 km and a 16-km layer at mean altitude of 8 km. For such a two-step model profile we also calculated the parameter δ_K. As evident from Table 2, the results obtained are not much different from real profiles.

It is likely that the turbulence profile corresponding to the instantaneous observing conditions will not be known precisely. Moreover, it rapidly changes because of turbulence intermittence. So an important issue is the sensitivity of wave-front reconstruction to exact profile shape. To investigate this, we use either the mean Paranal profile or the Hufnagel profile to compute the matrix coefficients and the optimized spatial filters. Then the real profile is used to estimate the expected rms reconstruction error. By the way, when doing this, we might obtain an error transfer function $G(\mathbf{f})$ greater than 1, owing to the profile's mismatch.

The results are also given in Table 2. As expected, the smallest δ is obtained when the profile and the reference coincide. However, the use of the mean profile or even the Hufnagel profile for optimum filter definition does not degrade the performance dramatically. We see that the use of average (instead of actual) profile increases δ_K by 10–20%, leading to the γ_K loss of the same amount.

5. TURBULENCE PROFILE MEASUREMENT

Usually the necessity to measure real-time atmospheric turbulence profiles is evoked in relation to MCAO, and

Table 1. Equivalent Thickness of a Uniform Layer for Different Numbers of Guide Stars

	Number of Guide Stars								
Ratio	1	2	3	4	5	6	7	8	9
δ_K/L	0.690	0.278	0.120	0.118	0.074	0.074	0.048	0.054	0.038

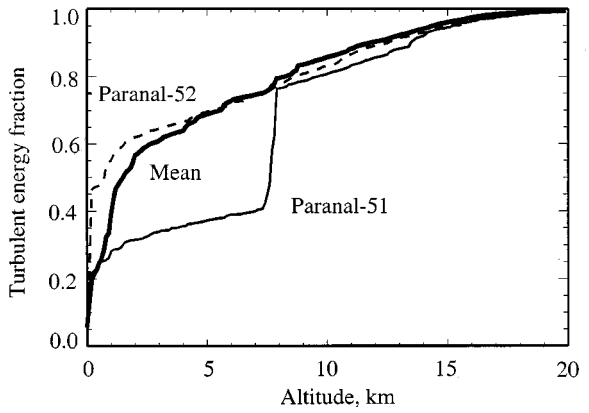

Fig. 4. Cumulative turbulence profiles for Paranal: fraction of total turbulent energy below a given altitude. Two different cases are selected: profile 52, which is similar to the mean profile (dashed and solid curves, respectively) and profile 51 (thin curve), which shows a strong peak at an altitude of 7.5 km, containing approximately 1/3 of the total energy.

Table 2. Equivalent Thickness of Atmosphere δ_K

Profile	Reference Profile	δ_3 (m)	δ_5 (m)
Hufnagel		889	554
Paranal mean		875	539
Paranal model		808	479
Paranal-51		972	572
Paranal-52		867	526
Paranal-51	Mean	1110	671
Paranal-51	Hufnagel	1125	714
Paranal-52	Mean	900	551
Paranal-52	Hufnagel	920	583

reference is made to the existing techniques such asSCIDAR (see the most recent SCIDAR description in Ref. 17). However, with WFS data on several NGS's, the profile can be obtained as a by-product, eliminating the need for an additional instrument.

The cross spectrum $W_{kk'}$ of two WFS signals S_k and $S_{k'}$ contains information on the profile. Starting from Eq. (4), neglecting noise (it is uncorrelated between two NGS's), and also using the expression Eq. (2) for phase Fourier transform, we have

$$W_{kk'}(\mathbf{f}) = \langle S_k S_{k'}^* \rangle = |\mathcal{M}|^2 \sum_{n=1}^{N} \langle \tilde{\phi}_n(\mathbf{f}) \tilde{\phi}_n^*(\mathbf{f}) \rangle \times \exp[-2\pi i \mathbf{f}(\boldsymbol{\theta}_k - \boldsymbol{\theta}_{k'}) h_n], \quad (28)$$

where the summation is performed over all N atmospheric layers that are mutually independent. Recognizing in the average phase product the phase power spectrum [Eq. (9)], replacing the sum with the integral, and performing altitude integration with the help of Eq. (13), we obtain the final expression:

$$W_{kk'}(\mathbf{f}) = |\mathcal{M}|^2 W_0(\mathbf{f}) \tilde{C}[\mathbf{f}(\boldsymbol{\theta}_{k'} - \boldsymbol{\theta}_k)]. \quad (29)$$

Instead of the cross spectrum, the cross-correlation function of WFS data may be calculated. Then it follows from backtransforming Eq. (29) that it equals the scaled turbulence profile convolved with some kernel that depends on the shape of W_0 and $\mathcal{M}$. The same is true for SCIDAR, except that its kernel function is different and altitude dependent, whereas Eq. (29) leads to a true convolution. For S–H WFS the kernel is equal to the slope covariance function, known to have a sharp peak and long wings. Of course, both SCIDAR and the profile measurement from WFS data are just particular cases of turbulence sensing with crossed beams, known for long time.

The maximum spatial frequency of the WFS data will be $1/2d$, where d is the S–H subaperture size (Nyquist condition). The maximum separation between NGS's will be $\sim 2\Theta$. This means that the altitude resolution of the profile will be of the order of d/Θ. Typically one might expect that $d \approx r_0$ and $\Theta \approx r_0/\delta_K$, so the vertical resolution will be not too different from δ_K.

Further details of profile measurement from WFS data (sensitivity, finite telescope-aperture diameter, deconvolution, etc.) are beyond the scope of this work.

6. NOISE PROPAGATION

The issue of noise propagation in turbulence tomography has not been clear until now. It has been suggested[4] that

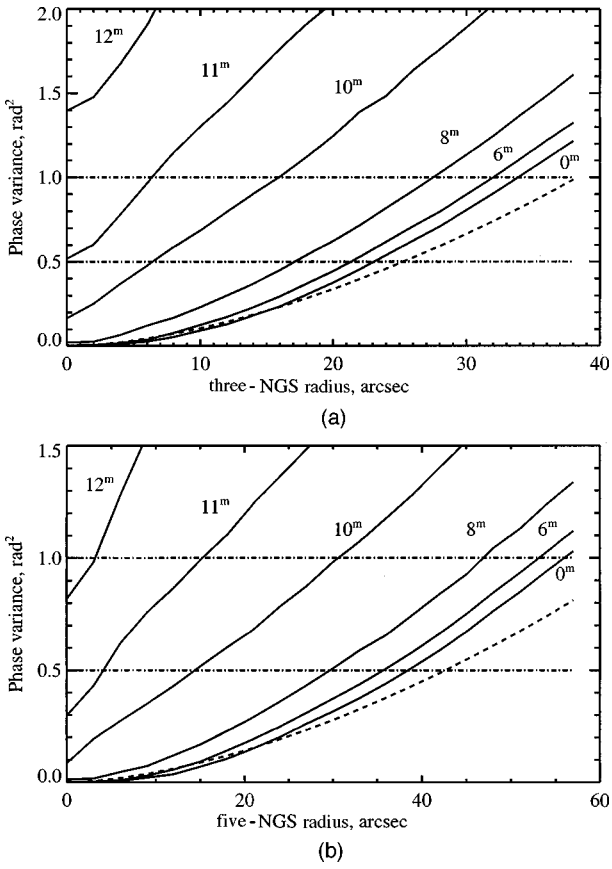

Fig. 5. Residual phase variance for a wavelength of 500 nm as a function of NGS configuration radius for (a) three NGS's and (b) five NGS's. Curves are labeled by NGS magnitudes. Dashed–dotted horizontal curves mark the rms residual levels of 0.5 and 1 rad^2, corresponding to the Strehl ratio degradation of 0.37 and 0.61, respectively. Dashed curves show the 5/3 scaling law [Eq. (26)]. The object is at the FOV center. A Paranal model profile with $r_0 = 0.15$ m is used.

each of the NGS's can be fainter than in conventional AO because their signals are used jointly for optimized wave-front estimation. However, the solution of an inverse problem (estimation of object phase from NGS phases) typically involves some noise amplification. In the above formalism, noise amplification can be traced to the fact that the modulus of the filters **g** exceeds 1 at some frequencies.

To study the noise propagation, a model of the S–H WFS was adopted with infinite spatial resolution (zero aperture size). We verified that for bright stars it yields exactly the same results as the $\mathcal{M} = 1$ model used in the previous sections. The parameters of S–H WFS were then chosen to compute photon flux from a given NGS magnitude (roughly, 1500 photons per square meter from a 10th-magnitude star), and spot size $\alpha = 1.5''$ was used. We do not pretend that these parameters correspond to some real AO system, and the NGS magnitudes given below must be considered as illustrative only.

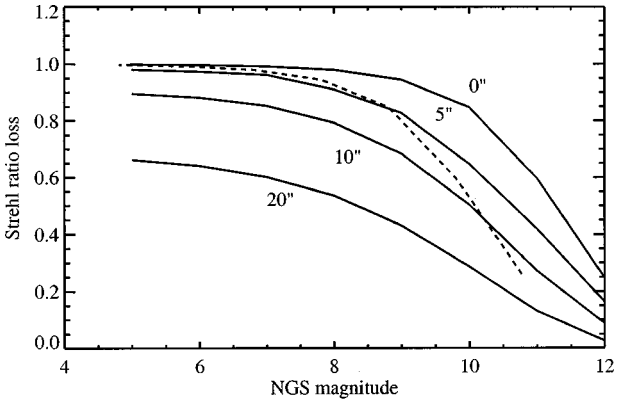

Fig. 6. Maximum Strehl ratio achievable at 500 nm as limited by combination of tomographic and photon noise errors with three NGS's, as a function of their magnitude. A model Paranal profile is used for calculation. The radius of the NGS configuration is indicated near the curves. The dashed curve shows for comparison an on-axis performance of a classic single-NGS AO system.

The rms residual phase variance at a wavelength of 500 nm was computed from Eq. (20) for the Paranal model profile with a typical median seeing of $r_0 = 0.15$ m. The object is placed at the FOV center. The limiting radius of NGS constellation γ_K (1 rad^2 variance) is 38.3″ and 64.5″ for three and five NGS's, as follows from the δ_3 and δ_5 values given in Table 2.

In Fig. 5 the phase variance at the FOV center is plotted against NGS configuration radius Θ for different NGS magnitudes (all NGS's are assumed to be equally bright and located at the vertices of a regular polygon). For bright NGS's these curves are close to the $(\Theta/\gamma_K)^{5/3}$ limit given by Eq. (26). The NGS separation corresponding to the 1 rad^2 error, however, is ≈10% less than predicted from the noise-free scaling law, even for 0^m NGS's. For fainter NGS's the variance increases, limiting the effective FOV size. It can be modeled as a sum of tomographic and photon noise contributions, but the photon noise level depends on the NGS separation.

In other words, our conclusion is that noise propagation cannot be neglected. With three or five 10^m NGS's located on axis ($\Theta = 0$), the wave-front error is well below

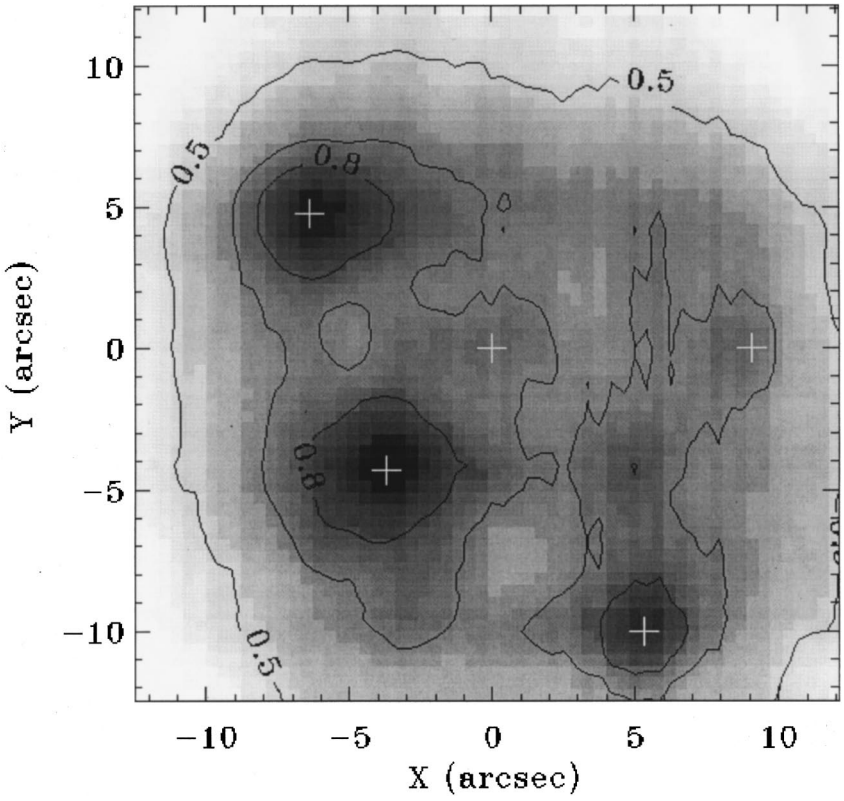

Fig. 7. Distribution of Strehl ratio at 500 nm over the FOV for a random constellation of five NGS's of magnitudes (from left to right) 7, 6, 11, 8, and 10 (NGS positions are marked by pluses). The faintest star is at the center. Paranal profile 51 was used. Contours with numbers indicate Strehl ratio levels.

$0.5\ \mathrm{rad}^2$. In agreement with common sense, on-axis error is inversely proportional to K, as can be inferred from Fig. 5. As soon as the NGS's are away from the FOV center, the photon noise increases roughly linearly with Θ. At larger NGS separations the photon noise curve will intercept the tomographic "5/3" curve, and the tomographic error will dominate. So, for the same NGS brightness and the same turbulence profile, the relative importance of photon noise with respect to tomographic noise depends on NGS separation. For 10th-magnitude stars in a 20″ field the photon noise dominates, but in a 120″ FOV, as appropriate for imaging in the infrared, the tomographic error would be larger than the photon noise, and such stars would be considered "bright."

It would be nice to model the tomographic noise propagation by a simple engineering formula such as Eq. (26). For the moment, however, we are not able to suggest a valid approximation. A very rough guess would be that the NGS's needed for tomography must be at least as bright as a single NGS for a classical on-axis AO. The comparison with classic AO is given in Fig. 6, showing the Strehl ratio at 500 nm as a function of NGS magnitude. The photon noise limit for a classic AO system is plotted by a dashed curve. With three NGS's there are three times more photons, so that when they are located on axis (no tomography), there is a gain of approximately 1 magnitude. However, for NGS separations of 10″ the curves intersect near 10th magnitude with a Strehl ratio of 0.5, indicating that there is no useful gain in limiting magnitude when reconstructing phase in a 10″ FOV.

In Fig. 7 an example of the maximum achievable (tomography-limited) Strehl ratio over FOV is shown for a random constellation of 5 NGS's of different magnitudes for a real Paranal turbulence profile. A Strehl ratio larger than 0.5 can be obtained over the whole 20″ FOV.

7. CONCLUSIONS

The limits of a linear tomographic phase reconstruction have been investigated. The effects of finite aperture diameter and incomplete beam overlap have been neglected as well as the additional problems inherent to laser guide stars. Our results hence describe the ultimate performance of a very large telescope with use of natural guide stars to measure the object phase. No errors due to correction (e.g., finite number of DM's, finite actuator spacing, finite bandwidth) are added, so our performance estimates would refer to a case when the wave front is corrected by an ideal DM for the selected object only.

Contrary to current belief, it has been shown that the minimum reconstruction error is dominated entirely by the continuously distributed turbulence component and that the presence of strong turbulent layers has little effect. The minimum error can be described by a new parameter δ_K, equivalent thickness of a turbulence profile. This thickness is estimated to be ~1 km and ~0.5 km for three and five NGS's, respectively, for some representative profiles, including the Hufnagel–Valley one. Thus the FOV radius of the future MCAO systems with a small number of guide stars is not expected to exceed $60''[\lambda/(500\,\mathrm{nm})]^{6/5}$. For an 8-m telescope the number of pixels along one axis in a Nyquist-sampled corrected image will be no more than a few thousand, whatever the wavelength.

The good news is that exact profile knowledge is not critical for wave-front reconstruction. A loss of FOV size resulting from the use of some model profile (instead of a true one) for optimum filter computation is quite moderate, typically within 10%. The profile itself can be extracted from the WFS data, eliminating the need to operate a special instrument for its real-time measurement.

Noise propagation in a tomographic reconstruction, like in any inverse problem, *is* significant. Thus the hope of using somewhat fainter NGS's for tomography are not justified. Faint NGS's must be closer to the object, all other parameters being equal. A tradeoff between magnitude and field size will be necessary in the study of the future MCAO systems with use of NGS's.

ACKNOWLEDGMENTS

This research has benefited from the support of the European Training and Mobility of Researchers program Laser Guide Stars for 8-m Class Telescopes. We are grateful to M. Le Louarn and R. Conan for comments on the manuscript. The comments of the two anonymous referees helped to improve the clarity of the article and are very much appreciated.

A. Tokovinin's e-mail address is atokovinin@ctio.noao.edu.

REFERENCES

1. R. H. Dicke, "Phase-contrast detection of telescope seeing errors and their correction," Astrophys. J. **198**, 605–615 (1975).
2. J. M. Beckers, "Increasing the size of the isoplanatic patch with multiconjugate adaptive optics," in *Proceedings of the ESO Conference on Very Large Telescopes and their Instrumentation*, M.-H. Ulrich, ed. (European Southern Observatory, Garching, Germany, 1988), pp. 693–703.
3. M. Tallon and R. Foy, "Adaptive telescope with laser probe: isoplanatism and cone effect," Astron. Astrophys. **235**, 549 (1990).
4. D. C. Johnston and B. M. Welsh, "Analysis of multiconjugate adaptive optics," J. Opt. Soc. Am. A **11**, 394–408 (1994).
5. B. L. Ellerbroek, "First-order performance evaluation of adaptive-optics systems for atmospheric-turbulence compensation in extended-field-of-view astronomical telescopes," J. Opt. Soc. Am. A **11**, 783–805 (1994).
6. T. Fusco, J.-M. Conan, V. Michau, L. M. Mugnier, and G. Rousset, "Phase estimation for large field of view: application to multiconjugate adaptive optics," in *Propagation through the Atmosphere III*, M. C. Roggemann and L. R. Bissonnette, eds., Proc. SPIE **3763**, 125–133 (1999).
7. A. Tokovinin, M. Le Louarn, and M. Sarazin, "Isoplanatism in a multiconjugate adaptive optics system," J. Opt. Soc. Am. A **17**, 1819–1827 (2000).
8. R. Ragazzoni, E. Marchetti, and G. Valente, "Adaptive-optics corrections available for the whole sky," Nature **403**, 54–56 (2000).
9. M. Le Louarn, N. Hubin, M. Sarazin, and A. Tokovinin, "New challenges for adaptive optics: extremely large telescopes," Mon. Not. R. Astron. Soc. **317**, 535 (2000).
10. F. Roddier, "The effects of atmospheric turbulence in optical astronomy," in *Progress in Optics*, E. Wolf, ed. (North-Holland, Amsterdam, 1981), Vol. XIX, pp. 281–376.
11. F. Rigaut, J.-P. Véran, and O. Lai, "An analytical model for Shack-Hartmann-based adaptive optics systems," in *Adap-*

tive Optical System Technologies, D. Bonaccini, ed., Proc. SPIE **3353**, 1038–1048 (1998).
12. W. H. Press, S. A. Teukolsky, W. T. Vetterling, and B. P. Flannery, *Numerical Recipes in C* (Cambridge U., Cambridge, UK, 1992), Chap. 13.3.
13. D. L. Fried, "Anisoplanatism in adaptive optics," J. Opt. Soc. Am. **72**, 52–61 (1982).
14. G. C. Valley and S. M. Wandzura, "Spatial correlation of phase-expansion coefficients for propagation through atmospheric turbulence," J. Opt. Soc. Am. **69**, 712–717 (1979).
15. A. Fuchs and J. Vernin, "Final report on PARSCA 1992 and 1993 campaigns," ESO Tech. Rep. VLT-TRE-UNI-17400-0001 (European Southern Observatory, Garching, Germany, 1996).
16. M. Sarazin, in *OSA/ESO Topical Meeting on Adaptive Optics*, M. Cullum, ed. (European Southern Observatory, Garching, Germany, 1996), pp. 439–444.
17. R. Avila, J. Vernin, and E. Masciadri, "Whole atmosphere profiling with a generalized SCIDAR," Appl. Opt. **36**, 7898–7905 (1997).